Article:
Senatore, EV, Taleb, W orcid.org/0000-0003-2179-7963, Owen, J et al. (4 more authors) (2018) Evaluation of high shear inhibitor performance in CO2-containing flow-induced corrosion and erosion-corrosion environments in the presence and absence of iron carbonate films. Wear, 405. pp. 143-152. ISSN 0043-1648

https://doi.org/10.1016/j.wear.2018.03.014

Evaluation of high shear inhibitor performance in CO_2-containing flow-induced corrosion and erosion-corrosion environments in the presence and absence of iron carbonate films

E. V. Senatore[1], W. Taleb[2], J. Owen[2], Y. Hua[2], J. A. C. Ponciano Gomes[1], R. Barker[2], A. Neville[2]

[1]Federal University of Rio deJaneiro-LabCorr, Rio de Janeiro, Brazil

[2]University of Leeds, Leeds, United Kingdom

Abstract

Carbon steel pipeline degradation occurs as a result of erosion-corrosion during oil and gas production. Sand particles contribute to this effect when they are present in conjunction with a high flow velocity. In carbon dioxide (CO_2) environments, and under certain conditions, the corrosion rate of the steel can be reduced by the formation of a protective iron carbonate ($FeCO_3$) layer. This work assesses the ability of $FeCO_3$ to protect the underlying steel in flow-induced corrosion and erosion-corrosion environments. Autoclave tests are performed at 60°C and 100 bar in a 1 wt.%NaCl CO_2-saturated solution for a duration of 48h to develop 60µm thick $FeCO_3$ films. The film-covered samples were then transferred into a submerged impinging jet (SIJ) apparatus to assess their ability to resist both flow-induced corrosion and erosion-corrosion environments at 25ºC and a flow velocity of 15 m/s (both with and without 1000 mg/L sand). Tests were also conducted in the presence of a commercially available corrosion inhibitor to evaluate the interaction. Results indicate that the $FeCO_3$ layer is able to considerably suppress corrosion of the carbon steel substrate. Experiments in the presence of both the $FeCO_3$ film and corrosion inhibitor demonstrated that there is a notable synergistic effect between these two components in providing resistance to erosion-corrosion.

Keywords: jet impingement; carbon dioxide corrosion; erosion-corrosion; iron carbonate; corrosion inhibitor

1. Introduction

The corrosion of carbon steel pipelines in carbon dioxide (CO_2)-containing environments is a common occurrence within the oil and gas industry [1]. Dissolved CO_2 within the brine component of production fluids permits the speciation of carbonic acid (H_2CO_3), which can result in the electrochemical dissolution of carbon steel due to its low corrosion resistance [2].

In addition to electrochemical dissolution, the presence of solid particles in conjunction with the corrosive production fluid can result in the pipeline material being subjected to erosive conditions as well as a corrosive environment [3]. This results in a degradation mechanism which is termed as 'erosion-corrosion'. Erosion–corrosion is a form of tribo-corrosion material loss mechanism caused by flowing fluid (typically in the presence of sand) degrading both the surface layer (e.g. passive films or corrosion products) and the base metal through a combination of mechanical removal and material dissolution. The synergistic effects between erosion and corrosion are well documented and can significantly exceed degradation rates compared to the sum of the individual processes acting separately [4-6].

A number of studies have examined the erosion-corrosion resistance of carbon steel in CO_2-containing environments [4,5,7]. These studies typically focus on quantifying the resistance of carbon steel in conditions where no corrosion product formation is anticipated, or consider the potential of corrosion inhibitors in mitigating not only steel dissolution, but in alleviating the erosion component of material loss. A number of studies have demonstrated that the action of the corrosion inhibitor can involve both the reduction of metal loss during mechanical erosion from particle impingement and suppression of active corrosion. Previous studies have also shown that corrosion inhibitors are able to adsorb onto the surface of sand particles. This can have the detrimental effect of reducing the bulk inhibitor concentration which influences the adsorption onto the steel surface [8]. However, it has been argued that the adsorption of inhibitors onto sand may be beneficial in terms of hindering their ability to cause erosion of the substrate [7,9]. The capability of these chemicals to lower electrochemical corrosion reactions and the mechanical damage associated with particle impingement is well documented, but the underlying mechanisms have been the subject of less attention [4].

As previously stated, a considerable amount of research has been directed towards understanding erosion-corrosion synergies for carbon steel in CO_2 environments in the absence and presence of corrosion inhibitors [4, 6-10]. This research typically focuses on conditions where corrosion product formation does not occur on carbon steel. However, the formation of iron carbonate ($FeCO_3$) is a common observation in CO_2-containing environments and readily precipitates onto the inner pipeline if a critical level of supersaturation is exceeded. The $FeCO_3$ layer can afford considerable corrosion protection to carbon steel by blocking active sites on the substrate surface, and developing a diffusion barrier to electrochemically active species [11]. Considering that this layer can develop to be the order of 10's or 100's of μm thick, there is the potential for it to mitigate the erosive effect generated by sand particle impingement. This paper focuses on addressing this knowledge gap by evaluating the effect of a 60μm thick $FeCO_3$ layer in its ability to withstand flow-induced corrosion and erosion-corrosion environments, both in the absence and presence of a commercially available corrosion inhibitor. The work initially assesses the flow-induced corrosion and erosion-corrosion performance of API 5L X65 carbon steel in the absence of an $FeCO_3$ layer, both with and without corrosion inhibitor using a submerged impinging jet (SIJ). Test conditions selected were a 3.5wt.%NaCl CO_2-saturated solution at 25°C, pH 4.7 and 15 m/s, with and without the presence of 1000 mg/L sand to create a flow-induced corrosion and erosion-corrosion environment, respectively. The experiments are then repeated under the exact same experimental conditions for a steel sample whereby an $FeCO_3$ film has been generated in advance on the steel surface at 100 bar and 60°C for 48h in a 1wt.%NaCl CO_2-saturated solution using an autoclave system.

In addition, the experiments are performed with and without the presence of corrosion inhibitor to determine the interaction with a wet-ground surface and a $FeCO_3$ filmed surface in each environment. Although testing of corrosion inhibitors is usually carried out so to avoid or delay the $FeCO_3$ protective layer, the inhibitor potency in the presence of an $FeCO_3$ partially or fully covering the steel also deserves attention and is mainly relevant for parts of pipelines where rapid formation of $FeCO_3$ is expected and/or there is intermittency in the injection of inhibitor which allows the film to develop [12]. Usually, it is assumed that the corrosion protection is achieved when the $FeCO_3$ is not yet developed while the corrosion inhibitor effect is negligible if the $FeCO_3$ film is already fully covering the steel surface, but contradictory conclusions at various conditions have already been uncovered [13].

Moreover the protection provided by the $FeCO_3$ when sand is produced is still not well defined.

2. Experimental setup and procedure

2.1 Materials and sample preparation

The material used in this study is an API 5L X65 carbon steel which is commonly employed in the oil and gas industry due to its adequate mechanical properties and low cost [14]. The steel possesses a ferritic-pearlitic microstructure and the elemental composition is provided in Table 1. The specimen geometry consists of discs with an exposed area of 4.9 cm^2 (25 mm diameter) to the electrolyte in all experiments. Surface preparation prior to SIJ or autoclave experiments consisted of wet-grinding the sample using 1200 grit silicon carbide abrasive paper before degreasing with acetone, followed by high purity ethanol and drying with compressed air.

Table 1: Elemental composition of API 5L X65 steel (wt.%)

C	Si	Mn	P	S	Cr	Mo	Ni
0.12	0.18	1.27	0.008	0.002	0.11	0.17	0.07
Cu	**Sn**	**Al**	**B**	**Nb**	**Ti**	**V**	**Fe**
0.12	0.008	0.022	0.0005	0.054	0.001	0.057	Balance

Samples used for SIJ mass loss measurements or $FeCO_3$ film-formation experiments in the autoclave were stored in a vacuum desiccator until required and weighed immediately before use on an electronic balance to within an accuracy of 0.01 mg. To obtain electrochemical measurements from carbon steel samples within the SIJ, wires were soldered to the back of the steel samples before mounting them in a non-conducting resin. In the case of the $FeCO_3$ filmed samples, the back of each disc was carefully ground in the absence of water before attaching the wire using conductive glue. The sample was then inverted in the mold on a holder and resin was injected carefully around the back and sides of the specimen until it reached a height just below the top of the $FeCO_3$ filmed surface. This resulted in one face of the sample being exposed to the jet, consistent with the mass

loss samples which were placed in holders to expose only one face of the sample to the jet with the aid of an O-ring seal.

2.2 Autoclave film-formation procedure

A selection of steel specimens were pre-filmed with $FeCO_3$ prior to insertion in the SIJ. The $FeCO_3$ layers developed on the surface were created by placing five of the 25 mm diameter samples within the autoclave, generating a total surface area of ~24.5 cm^2 exposed to 200 ml of solution.

With regards to the autoclave procedure, the prepared 1 wt.%NaCl solution used in each experiment was de-aerated with CO_2 in a separate container for a minimum of 12 h prior to use. Specimens were then suspended inside the autoclave on non-conducting wires whilst ensuring they were not in contact with one another or the walls of the autoclave to eliminate galvanic effects. The prepared, CO_2-saturated solution was then delivered into the autoclave at ambient temperature and pressure before sealing. All lines to the vessel, as well as the vessel itself were then purged with CO_2 and evacuated multiple times to ensure removal of CO_2 within the system. Additional CO_2 was then transferred into the autoclave before it was heated and pressurised to the correct temperature and pressure (100 bar and 60°C in this instance). The starting point of the experiment was taken from the point at which the operating conditions were reached in the autoclave, with experiments running for a total of 48 h.

2.3 Flow-induced corrosion and erosion-corrosion experiments

The SIJ used for erosion-corrosion testing shown in Figure 1 consisted of a reservoir with a 50 L capacity, which was filled with the test solution and recirculated through a dual nozzle arrangement before impinging onto two specimens set at a distance of 5mm below the exit of the nozzles at a velocity of 15 m/s. The flow velocity was measured at the exit of the 4mm diameter nozzles and calibrated prior to starting the test. The temperature of the solution was maintained at 25°C throughout the entire experiment.

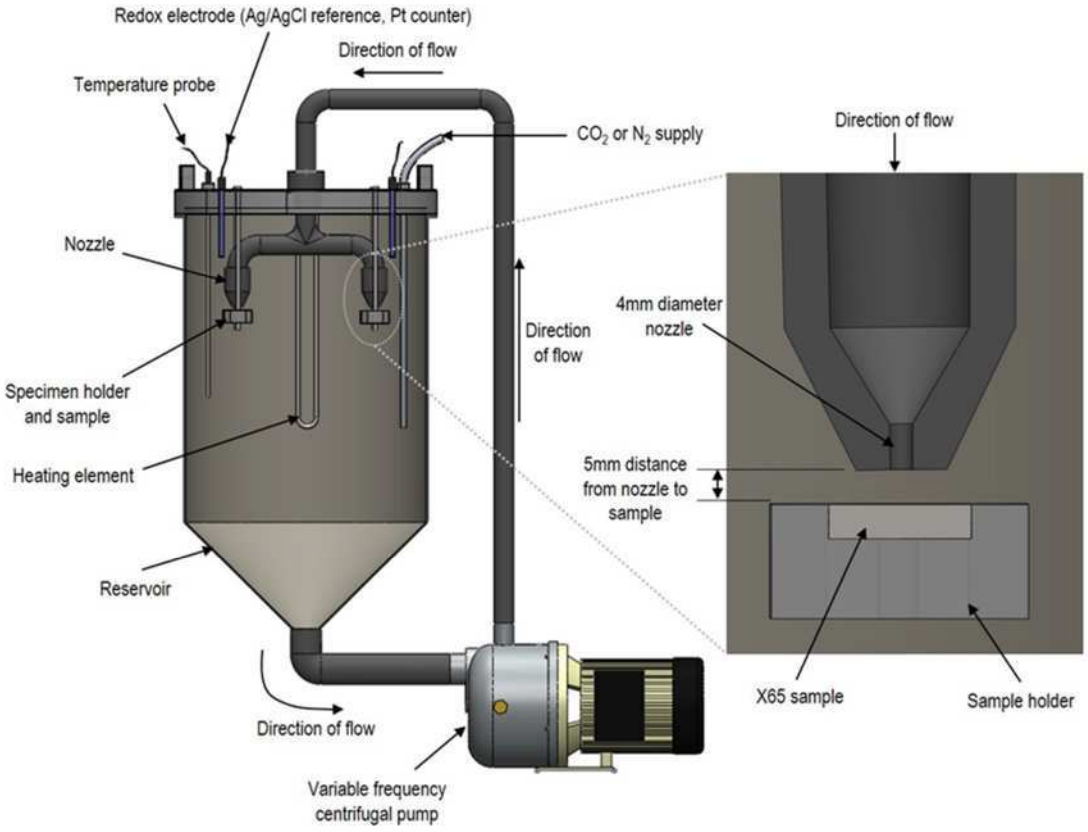

Figure 1: The submerged impingement jet (SIJ) apparatus used for flow-induced corrosion and erosion-corrosion testing

Two types of experiments were performed in this study; flow-induced corrosion (in the absence of sand) and erosion-corrosion (in the presence of sand particles). For both experiments, CO_2 was bubbled into the 50 L, 3.5 wt.%NaCl solution for a minimum of 12 h to reduce the dissolved oxygen concentration. Both mass loss samples and electrochemical samples were placed in customised holders which ensured that only one face of the sample (with an exposed area of 4.9 cm^2) was exposed to the electrolyte within the rig. Prior to starting the SIJ experiment, samples were placed into the holders and lowered into the rig. The system was then sealed with the exception of an outlet hole through which CO_2 could escape as the system was continuously purged with CO_2 throughout the experiment to prevent oxygen ingress. For erosion-corrosion experiments, 1000 mg/L of sand was added to the system. The sand particles possessed a mean diameter of ~250 µm, with an image of the particles provided in Figure 2. For all erosion-corrosion experiments, the sand was added to the system after the pump was started to ensure an even distribution of sand particles throughout the rig. A fresh supply of sand was used in every experiment to ensure consistent results.

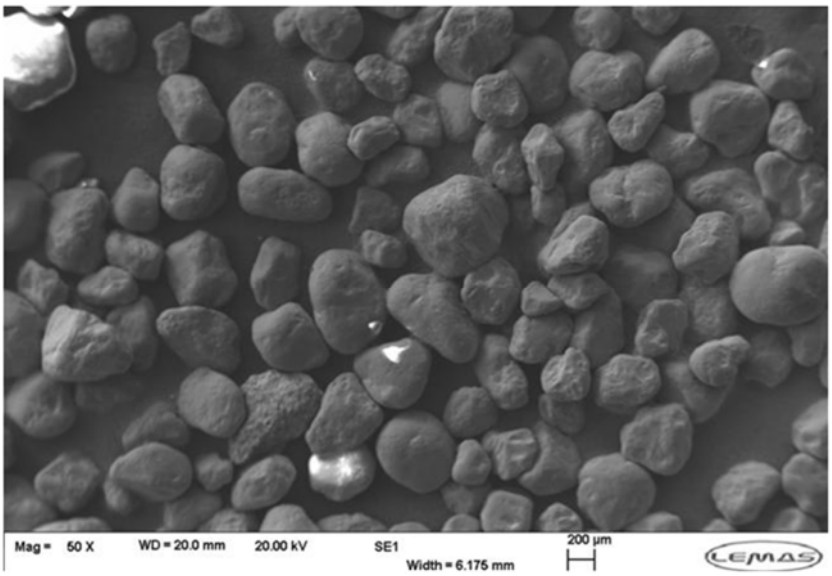

Figure 2: SEM images of HST60 sand particles used in this study; mean diameter is ~250 µm

Both flow-induced corrosion and erosion-corrosion experiments were performed in a 3.5 wt.%NaCl solution set at a pH of 4.7 and temperature of 25℃, with a flow velocity of 15 m/s exiting the nozzle. Flow-induced corrosion tests were conducted on wet-ground and $FeCO_3$ pre-filmed samples in the absence and presence of 100 ppm corrosion inhibitor for a total of 6h. The same experimental matrix was utilised in erosion-corrosion environments.

In relation to the application of corrosion inhibitor, a commercial high shear CO_2 corrosion inhibitor was used in this study at a concentration of 100 ppm. The chemical package is based on a combination of 2-butoxyethanol, quaternary ammonium compounds and amines. Corrosion inhibitor was added once the pump started to ensure thorough mixing of the inhibitor in the system. The open circuit potential (OCP) of the steel was then monitored and allowed to stabilise for 5 mins before electrochemical measurements commenced.

The full set of experiments is provided in Table 2 for clarity to summarise the entire test matrix.

Table 2: Summary of test conditions evaluated using the submerged impinging jet (SIJ)

Material and Operating conditions	Corrosion Inhibition	Flow Regime	Sand Concentration	Initial surface conditions of sample
API 5L X65 steel, 25℃, 15 m/s pH 4.7 3.5 wt.% NaCl 90° impact angle 6h duration	No corrosion inhibitor	Flow-induced corrosion	0 mg/L	Wet-ground surface
				$FeCO_3$ pre-filmed surface
		Erosion-corrosion	1000 mg/L	Wet-ground surface
				$FeCO_3$ pre-filmed surface
	100 ppm corrosion inhibitor	Flow-induced corrosion	0 mg/L	Wet-ground surface
				$FeCO_3$ pre-filmed surface
		Erosion-corrosion	1000 mg/L	Wet-ground surface
				$FeCO_3$ pre-filmed surface

2.4 Corrosion rate determination using mass loss and electrochemical measurements

The evaluation of the degradation rate was conducted using a combination of mass loss and electrochemical measurements. Mass loss measurements were conducted on erosion-corrosion samples while electrochemical measurements were performed on both erosion-corrosion and flow-induced corrosion samples. After 6 h of exposure, the mass loss samples were removed from the rig, cleaned with Clarke's solution (20 g antimony trioxide + 50 g stannous chloride + 1000 ml 38% hydrochloric acid) in accordance with ASTM Standard G1-03[15], rinsed with distilled water, dried with compressed air and weighed to determine the mass loss.

Electrochemical measurements involved the use of the Linear Polarisation Resistance (LPR) technique which was implemented to provide a general corrosion rate across the entire steel surface. The SIJ was integrated with a three electrode cell which comprised of a

working electrode, a platinum auxiliary electrode and a Ag/AgCl reference electrode. The LPR measurements were performed over the first 4.5 h of the 6 h experiment. This consisted of scanning from 15mV more negative than the open circuit potential (OCP) of the steel sample to 15mV more positive than OCP at a scan rate of 0.333 mV/s. After LPR measurements were complete, potentiodynamic polarisation sweeps were conducted by performing anodic or cathodic scans. This consisted of polarising each sample from OCP to either +300 mV or –500 mV vs the OCP at a scan rate of 0.333 mV/s, completing the 6 h test duration. AC impedance was used in a frequency range of 20,000Hz to 0.1 Hz purely to measure the solution resistance (R_s) which was used in conjunction with the polarisation resistance determined from the LPR method to enable the charge transfer resistance (R_{ct}) to be determined using Equation (1):

$$R_{ct} = R_p - R_s \tag{1}$$

The corrosion current density, i_{corr}, could then be calculated using Equation (2), taking into account the measured anodic and cathodic Tafel constant determined at the end of each experiment:

$$i_{corr} = \frac{B}{R_{ct}} = \frac{1}{R_{ct}} \frac{\beta_a \beta_c}{2.303(\beta_c - \beta_a)} \tag{2}$$

where B is the Stern-Geary coefficient, β_a is the anodic Tafel constant and β_c is the cathodic Tafel constant. The general corrosion rate is then calculated from Equation (3):

$$CR = 3.27 \frac{\mathrm{EW}. i_{corr}}{\rho} \tag{3}$$

Where CR is the corrosion rate in mm/year, EW is the equivalent weight of steel (which is equal to the molecular weight of steel (55.847g/mol) divided by the number of electrons involved in the corrosion process (2)), ρ is the density of the steel in g/cm^3 and 3.27 is a conversion factor.

2.5 Surface analysis

SEM was performed on samples using a Carl Zeiss EVO MA15 SEM to evaluate the morphology and coverage of corrosion products on the sample surfaces. All images were collected at a working distance of approximately 8mm with an accelerating voltage of 20 kV.

Samples were profiled using a Bruker NPFLEX white light interferometer. 3D profiles of the surfaces after each test were measured using this technique to compare the material loss as a result of the impacts from sand particles.

X-ray diffraction (XRD) measurements were performed on a Panalytical X'pert multipurpose diffractometers with a voltage of 40 kV and an intensity of 40 mA using dual Cu $K\alpha_{1+2}$ radiations with 10×10 mm programmable divergence slits.

3. Results and discussion

3.1 Flow-induced corrosion and erosion-corrosion behaviour of wet ground samples

3.1.1 Electrochemical and mass loss results of wet-ground samples

Initial tests were conducted in the absence of the pre-formed$FeCO_3$ film in flow-induced corrosion and erosion corrosion environments, both with and without the addition of corrosion inhibitor to enable comparison with the tests when the$FeCO_3$ corrosion product was present. From these full results, it is possible to assess the role of the $FeCO_3$ film and its synergistic or antagonistic behaviour with the corrosion inhibitor.

Figure 3 compares the corrosion rates calculated from LPR measurements in the absence and presence of sand and corrosion inhibitor both individually and collectively. Table 3 presents the Stern-Geary coefficients (B) applied for the calculation of corrosion rate using the LPR data. It should be stressed here that the analysis of the LPR technique and its representation in Figure 3 assumes a uniform dissolution rate across the entire surface of the steel sample. Based on profilometry analysis of samples subjected to flow-induced corrosion conditions, no wear profile existed, indicating no significant accentuation of dissolution rate at the centre of the sample due to the differing flow characteristics across the diameter of the sample. Given that the *in situ* corrosion rate in uninhibited erosion-corrosion conditions was only marginally greater than in flow-induced corrosion, this suggests that the plastic deformation created at the centre of the sample has little effect, if

any, in terms of enhancing the corrosion rate locally. As for erosion-corrosion experiments in the presence of inhibitor, it cannot be disputed that the corrosion rate at the centre of the sample is likely to be enhanced due to the successive sand particle impacts which can remove the inhibitor film, so the average LPR response for this sample in Figure 3 should be interpreted with caution. This is also for the case with the interpretation of results later in this paper with the use of $FeCO_3$ pre-filmed samples.

Nonetheless, referring to Figure 3, it is clear that the inhibitor is effective in reducing corrosion rate regardless of whether the sand erosive counterpart is present or not. Application of the corrosion inhibitor reduces the LPR corrosion rate from approximately 4.9 ± 0.01 to 0.08 mm/year when no sand is present and from 5.5 ± 0.01 to 0.2 mm/year when the abrasive particles are added. Thus, the damage associated to corrosion of API 5L X65 steel can be decreased by 98% when the corrosion inhibitor is injected at 100 ppm with no sand and 96% when sand particles are present.

This reduction in inhibitor efficiency with regards to the corrosion component of material loss is likely to be associated with impingement of sand onto the steel surface causing periodic removal of the inhibitor film so as to expose the specimen's surface and allow further dissolution before the re-forming of the protective layer. Furthermore, from previous work it is clear that some of the active compounds within the inhibitor are able to adhere to the sand particles themselves, reducing the available inhibitor concentration in the bulk solution [8].

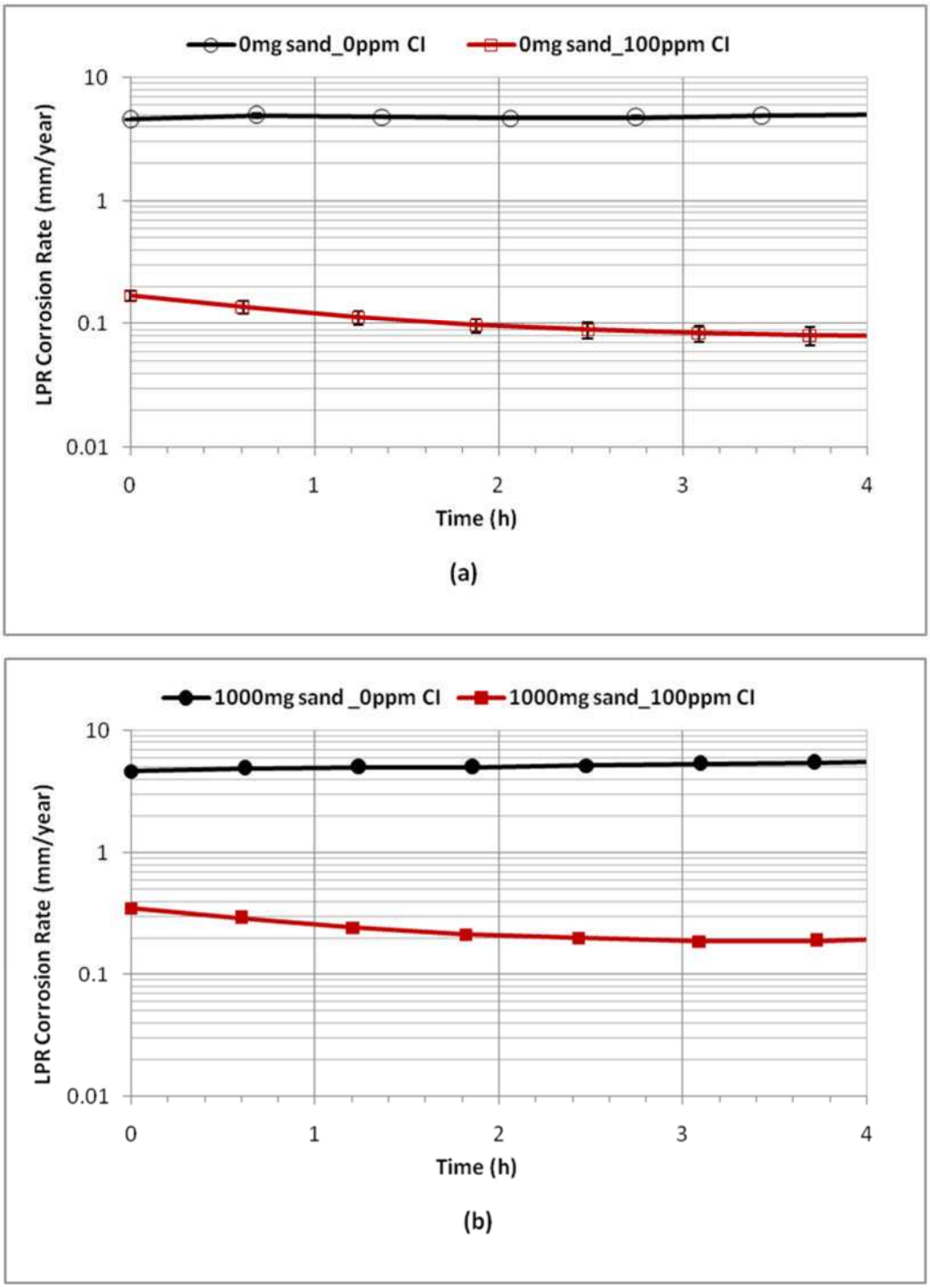

Figure 3:LPR corrosion rates of API 5L X65 as a function of time for wet-ground samples exposed to (a) flow-induced corrosion and (b) erosion-corrosion conditions; experiments are in the presence and absence of 100 ppm corrosion inhibitor (CI) and 1000 mg/L sand; test conditions are 15 m/s, 25℃ and pH 4.7in a 3.5 wt.%NaCl solution CO_2-saturated at 1bar total pressure.

Table 3: Stern-Geary coefficients used in blank and inhibited flow-induced corrosion and erosion-corrosion tests

	0mg/L sand 0ppm corrosion inhibitor	0mg/L sand 100ppm corrosion inhibitor	1000mg/L sand 0ppm corrosion inhibitor	1000mg/L sand 100ppm corrosion inhibitor
Stern-Geary coefficient (B) mV/decade	24.92	23.78	25.17	23.33

The total mass loss values expressed for the erosion-corrosion tests in the presence and absence of inhibitor for initially wet-ground steel samples are provided in Figure 4. This total degradation rate can be attributed to the summation of four different material loss components [9] as shown in Equation(4):

$$TML = E + C + dE_C + dC_E \quad (4)$$

where TML is the total mass loss, E is pure erosion in the absence of corrosion and C is the corrosion in the absence of erosion, dC_E is the effect of erosion on corrosion and dE_C is the effect of corrosion on erosion [9]. The combination of dE_C and dC_E is termed as the synergistic effect which is the factor responsible for producing degradation rates greater than the summation of the erosion and corrosion rates acting individually.

From the data collected in erosion-corrosion conditions, it is possible to determine the contribution of the corrosion component (C + dC_E) through the application of *in situ* electrochemistry and the erosion component (E +dE_c) using the total mass loss in conjunction with the corrosion component. The contribution of these components is reflected in Figure 4 in the absence and presence of 100 ppm corrosion inhibitor.

Considering the components of material loss in Figure 4, in blank tests there is a corrosion dominant environment since the corrosion damage (C+dC_E) makes up ~70% of the total degradation rate. The addition of inhibitor was able to reduce the damage attributed to corrosion from 70% to 21% at 25℃ while the percentage contribution from the erosion component increased because of the suppression of the active corrosion process. The application of the inhibitor is able to reduce the total erosion-corrosion rate by 86%, while the corrosion component is reduced by 96%. The inhibitor also has a role in reducing the

erosion component of material loss. Several theories have been identified to explain this, including the role of inhibitor adsorption onto sand particles [8, 16] and surface which influences impact velocity/energy, but also the fact that the lack of corrosion produces a work-hardened layer at the impingement location which provides more resistance to the erosion processes at shallow impact angles [17].

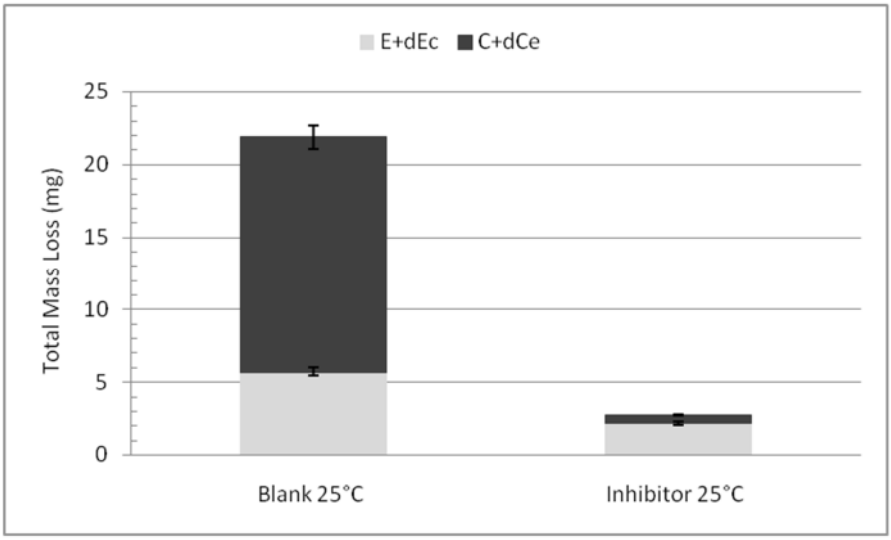

Figure 4: Erosion-corrosion degradation rates of wet-ground X65 carbon steel expressed as erosion and corrosion components with and without the application of 100 ppm corrosion inhibitor. Test conditions: 15 m/s, 25℃, pH 4.7, 1000 mg/L sand in a CO_2-saturated 3.5 wt.%NaCl solution at 1bar total pressure for 6 h.

The surface profile of the two erosion-corrosion samples is provided in Figure 5. The two profiles show similar penetration depths, with the inhibited test exhibiting greater loss at the very centre of the sample compared to the surrounding area. With regards to each sample, the original height of the entire surface needs to be considered as this will be greater for the uninhibited sample as a result of the significant corrosion process. Based on the LPR corrosion rates, the difference in corrosion rates of ~5-5.3 mm/year equates to a thickness loss of the surrounding area of ~4 µm, meaning that the penetration depth of each sample are very similar. This is important as it indicates that for direct impingement, the addition of inhibitor fails to alleviate the penetration depth at the maximum point, despite considerably reducing the overall level of degradation.

According to Barker et al. [4], a potential increase in penetration depth in the presence of inhibitor could be associated with the role of the inhibitor on the corrosion process, as a certain degree of plastic deformation would be necessary to facilitate or encourage material removal at high impact angles at the centre of the sample. It is expected that the high

corrosion rate in the blank tests could reduce the extent of plastic deformation on the surface, thus reducing the level of material removal from erosion. Using inhibitor results in a reduction in corrosion rate at the centre of the specimen, leaving the material exposed to more plastic deformation, so more material could potentially be removed at the sample centre. However, based on these results the depths of penetration are comparable and in this scenario, the effect had not been observed to any great extent.

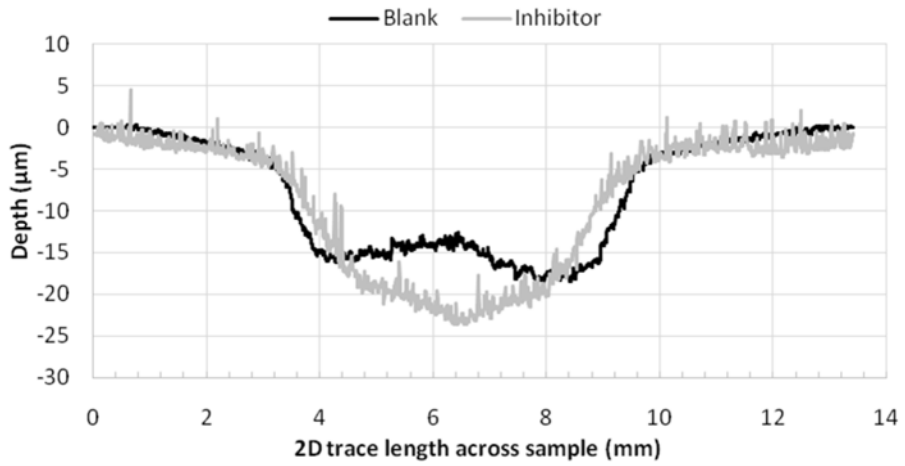

Figure 5: 2D profiles for API 5L X65 erosion-corrosion samples after cleaning. Tests are with and without the application of 100 ppm corrosion inhibitor on initially wet-ground X65 steel samples. Test conditions: 15 m/s, 25℃, pH 4.7, 1000 mg/L sand in a CO_2-saturated 3.5 wt.%NaCl solution at 1 bar total pressure.

3.1 Flow-induced corrosion and erosion-corrosion behavior of $FeCO_3$ pre-filmed samples

3.1.1 Development and analysis of $FeCO_3$ layer

Figure 6 indicates the top view and cross-section of the developed $FeCO_3$ layer after exposure to the CO_2-saturated 1 wt.%NaCl solution at 60°C and 100 bar for 48 h. The corrosion product layer is homogeneous in nature, covering the entire steel surface with a relatively uniform thickness of 60 µm. These conditions were chosen to ensure rapid development of a thick layer in a short time frame which still possessed the visual characteristic of $FeCO_3$ films which precipitate at lower pressure over extended periods of time [18]. In addition, the generation of the corrosion product film under these conditions is highly reproducible. The XRD pattern provided in Figure 7 confirms that the crystalline corrosion product observed is $FeCO_3$.

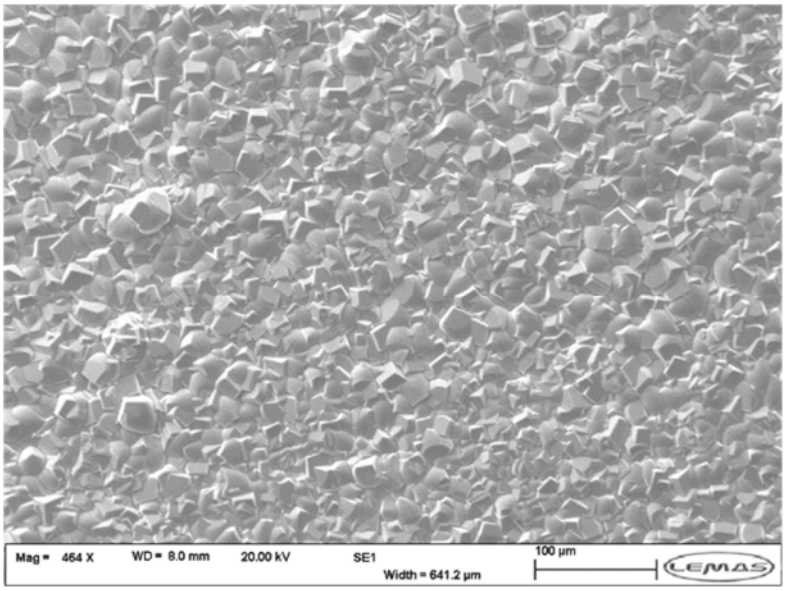

(a)

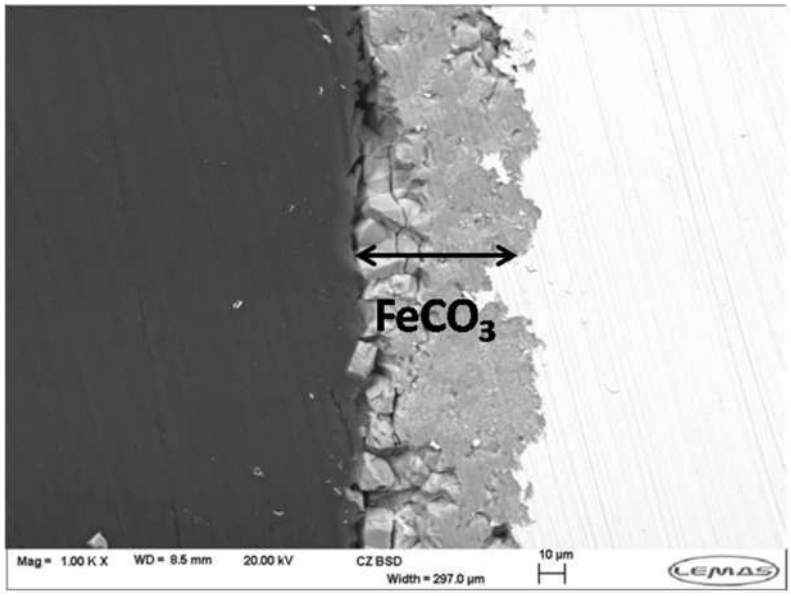

(b)

Figure 6: SEM images indicating (a) top view and (b) cross-section view of the developed $FeCO_3$ films on top of an API 5L X65 steel sample after exposure to a CO_2-saturated 1 wt.%NaCl brine at 60°C and 100 bar for 48 h.

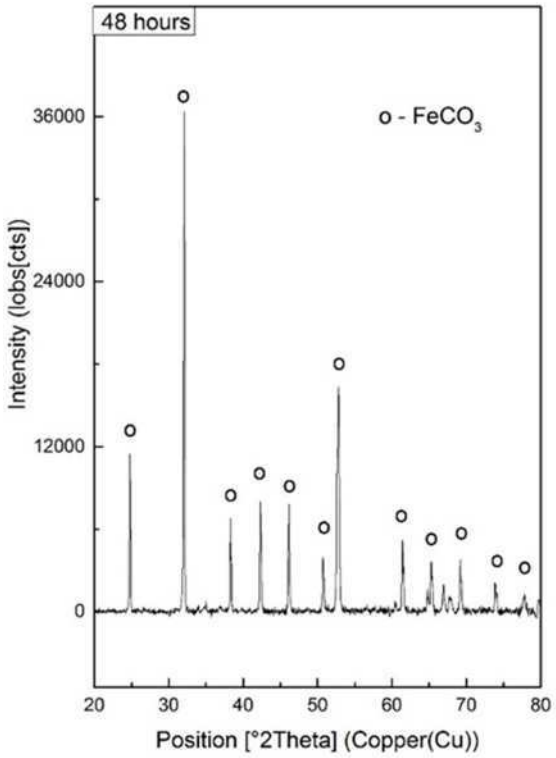

Figure 7: XRD pattern of API 5L X65 sample shown in Figure 6 confirming the crystalline phase as $FeCO_3$

3.1.1 Electrochemical and mass loss results of $FeCO_3$ pre-filmed samples

After the pre-formation of $FeCO_3$ on the metal surface, specimens were evaluated in flow-induced corrosion and erosion-corrosion environments. Figure 8 shows the LPR corrosion rates obtained for each environment, both in the absence and presence of corrosion inhibitor. In the flow-induced corrosion environment (Figure 8(a)), the sole presence of the $FeCO_3$ layer assists in reducing the corrosion rate by 96% from that in a blank system without inhibition (from 4.9 to 0.2 mm/year), the addition of the corrosion inhibitor when the $FeCO_3$ is already present reduces the corrosion rate further to 0.07 mm/year. This is marginally, yet not significantly lower than the corrosion rate with inhibition in the absence of the $FeCO_3$ layer (0.08 mm/year shown in Figure 3). However, the results demonstrate the inhibitor is able to penetrate through and work in conjunction with the pre-formed $FeCO_3$ layer. The protection is provided by the film acting as both a diffusion barrier for cathodic species and also by covering portions of the steel surface and blocking the iron dissolution reaction. It is clearly demonstrated in these experiments, that in a flow-induced

environment, the $FeCO_3$ layer developed in this study expresses a similar level of efficiency in terms of supressing general corrosion compared with chemical inhibition.

Figure 9 shows SEM images of the steel surface in each of the flow-induced corrosion tests with the pre-filmed sample (both with and without inhibitor). At the centre of the sample in the absence of inhibitor (Figure 9(a)), signs of $FeCO_3$ removal were evident. It is not clear whether this was chemical dissolution or as a result of the hydrodynamic forces present due to turbulent effects from the fluid flow. Towards the outer edge of the sample in the absence of inhibitor (Figure 9(b)), no significant disruption to the $FeCO_3$ layer was observed. Addition of 100 ppm inhibitor appeared to protect the $FeCO_3$ from removal, with no noticeable difference being evident between the centre of the sample under direct impingement (Figure 9(c) showing a typical image), and the regions further towards the outer edge of the sample. This suggests that the inhibitor is able to improve the resistance of the $FeCO_3$ layer to either hydrodynamic removal, chemical dissolution or both.

Figure 8(b) shows the *in situ* corrosion rate as a function of time for erosion-corrosion tests on the pre-formed $FeCO_3$ film, both in the presence and absence of 100 ppm inhibitor. Here, a dramatic difference is observed in the corrosion component of mass loss for the $FeCO_3$ layer in the absence of inhibitor compared to the flow-induced corrosion environment. The pre-formed layer is still able to suppress corrosion, however, it is much less efficient in the presence of sand impingement, with the corrosion rate averaging ~0.7 mm/year, a reduction of 87%. This value is still much lower than the corrosion rate in the absence of $FeCO_3$ (5.5 mm/year), however, not as low as in the same environments with no sand present (0.2 mm/year). The combination of inhibitor and $FeCO_3$ layer generates adequate resistance to the corrosion component of degradation in the erosion-corrosion environment, reaching an *in situ* corrosion rate of 0.1 mm/year, which is lower than the corrosion rate of the wet-ground sample subjected to erosion-corrosion conditions with inhibitor (0.2 mm/year).

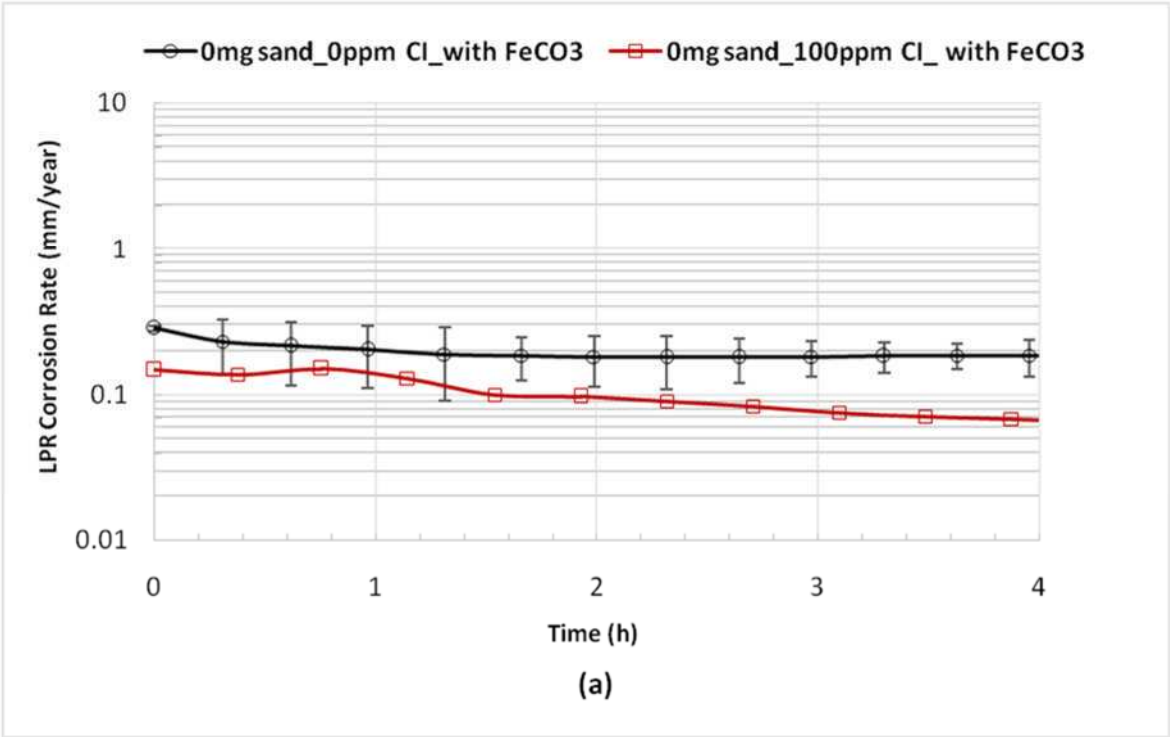

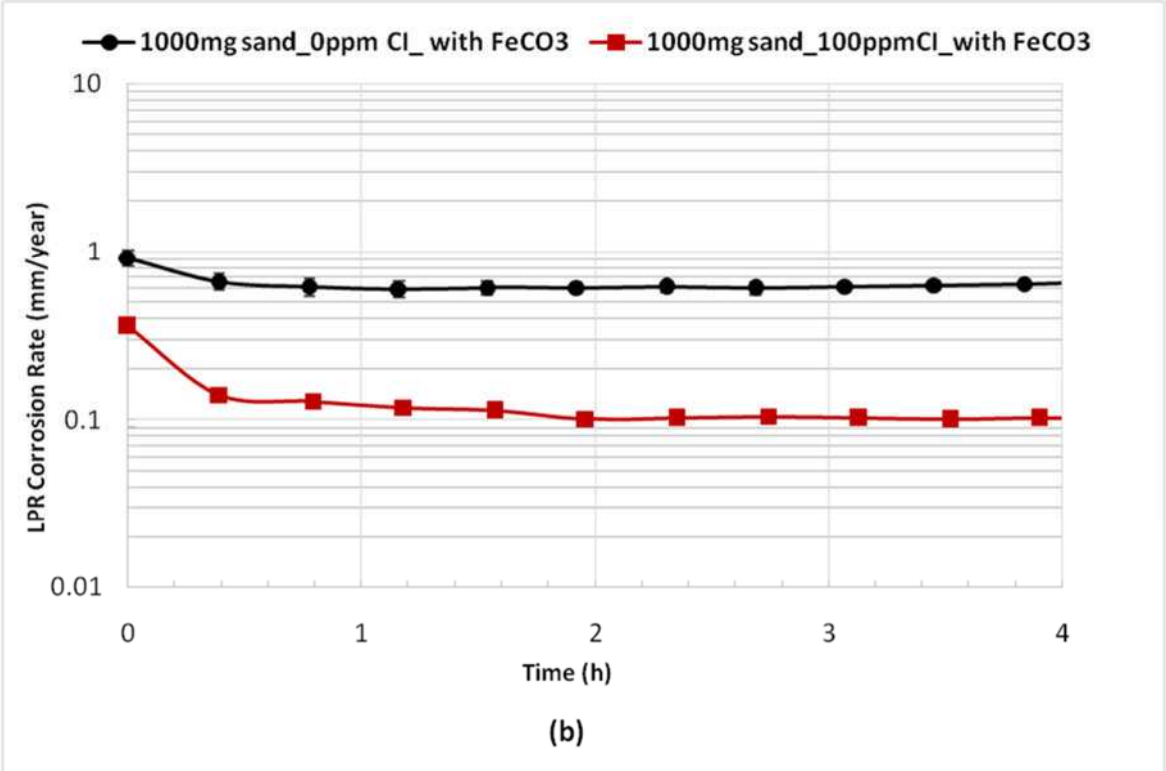

Figure 8: LPR corrosion rates of API 5L X65 as a function of time for $FeCO_3$ pre-filmed samples exposed to (a) flow-induced corrosion and (b) erosion-corrosion conditions; experiments are in the presence and absence of 100 ppm corrosion inhibitor (CI) and 1000 mg/L sand; test conditions are 15 m/s, 25℃ and pH 4.7in a 3.5 wt.%NaCl solution CO_2-saturated at 1bar total pressure.

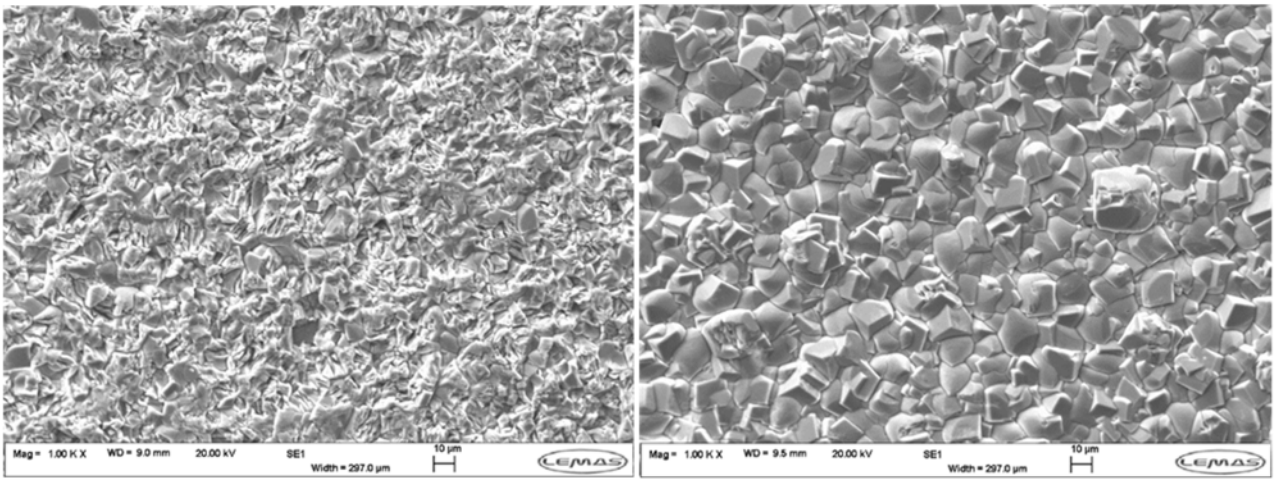

(a) **(b)**

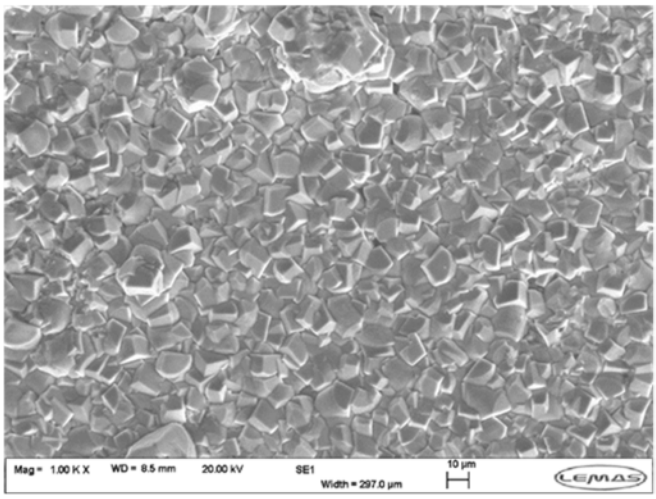

(c)

Figure 9: SEM images of (a) centre of sample under direct impingement in flow-induced corrosion environment with 0 ppm inhibitor, (b) outer region of sample in flow-induced corrosion conditions with 0 ppm inhibitor and (c) typical image of centre/outside of sample in flow-induced corrosion environment with 100 ppm inhibitor (no noticeable difference between the two regions); test conditions are 15 m/s, 25℃ and pH 4.7in a CO_2-saturated 3.5 wt.% NaCl solution at 1bar total pressure.

In the erosion-corrosion environment, the effect of sand particle impingement can produce significant levels of erosion in conjunction with corrosion. Figure 10 shows the erosion-corrosion resistance of the $FeCO_3$ layered surface in the presence and absence of inhibitor. As before, these have been divided into erosion and corrosion components based on consideration of total mass loss and the LPR response. The sole $FeCO_3$ layer is able to considerably suppress the corrosion component of degradation in the erosion-corrosion

environment but the erosion component is relatively high and it results in a total erosion-corrosion rate similar to tests in the absence of inhibitor and $FeCO_3$ layer (Figure 4).

In presence of 100 ppm inhibitor, the tendency remains the same. Only the corrosion component is reduced when it is compared with erosion-corrosion rate in blank tests in the absence of the $FeCO_3$ layer (Figure 4). However, it is important to note that the erosion component of damage here includes removal of the $FeCO_3$ layer (either by chemical or mechanical effects) in addition to damage to the substrate.

Considering the results in Figure 10, the inhibitor in conjoint with $FeCO_3$ layer plays a role in reducing not only the corrosion component of material loss, but also the erosion component from the blank system with the pre-filmed sample.

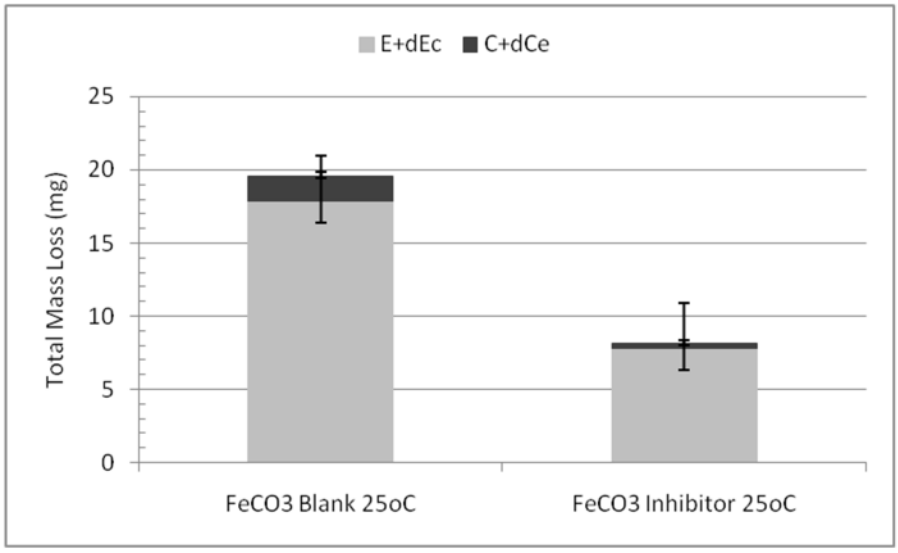

Figure 10: Erosion-corrosion degradation rates of X65 carbon steel samples pre-filmed with $FeCO_3$ expressed as erosion and corrosion components with and without the application of 100 ppm corrosion inhibitor. Test Conditions: 15 m/s, 25℃, pH 4.7, 1000 mg/L sand in a CO_2-saturated 3.5 wt.%NaCl solution at 1 bar total pressure for 6 h.

The surface morphologies of filmed samples after erosion-corrosion tests were observed by scanning electron microscopy (SEM). Figure 11 shows the centre (Figure 11(a)), transition region (11(b)) and edge (11(c)) of the sample subjected to erosion-corrosion in the absence of inhibitor, while Figures 11(d) to (f) depict the surface of the erosion-corrosion samples in the presence of inhibitor. Figures 11(a) and (d) indicate full removal of the film at the centre of impingement. However, the transition region between the centre and outside of the sample indicates that the inhibitor is able to provide added protection to the $FeCO_3$ layer as there are less regions of local removal of the film.

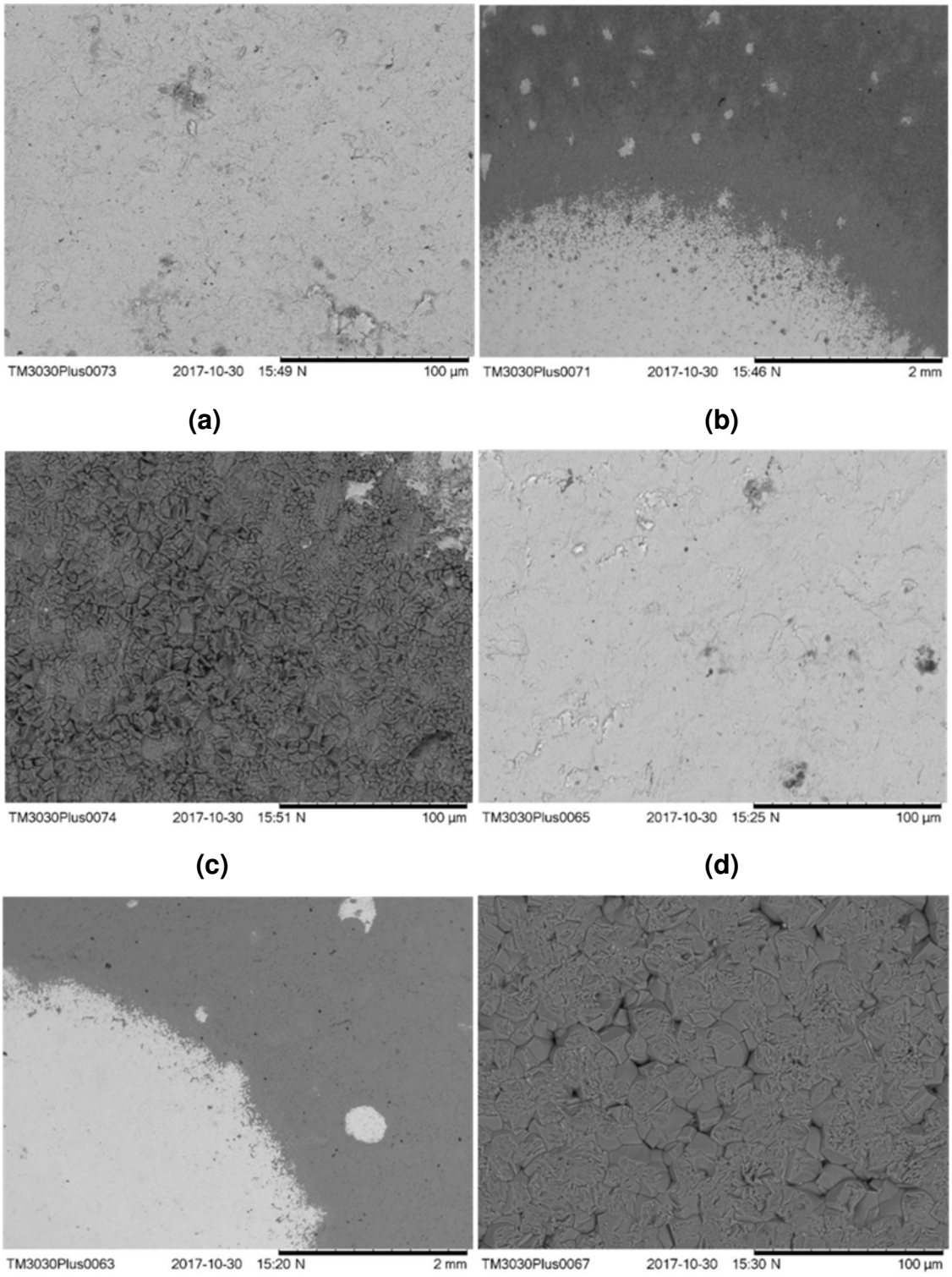

Figure 11:SEM images of (a) centre (b) transition region, (c) edge of the sample in erosion-corrosion environment with 0 ppm inhibitor and (d) centre (e) transition region and (f) edge of the sample in erosion-corrosion environment with 100 ppm inhibitor; test conditions are 15 m/s, 25℃ and pH 4.7 in a CO_2-saturated 3.5 wt.%NaCl solution at 1bar total pressure.

The SEM images indicate that the degradation of the sample is not uniform across the entire steel surface. Consequently, the assumed uniform degradation rates discussed previously could be somewhat misleading in terms of identifying the extent of damage caused to the steel surface. What effectively needs to be considered is the penetration depth and geometry of the wear scar generated from the impingement process. To address this issue, profilometry measurements were performed on the steel surface after removal of the corrosion product. The profiles are provided in Figure 12 and illustrate that the $FeCO_3$ layer is able to suppress the penetration depth from ~20 µm to less than ~10µm. This indicates that the $FeCO_3$ layer does provide some initial protection. However, the 60 µm layer was completely removed by direct impingement in the centre of the same after 6 h of exposure, limiting its effectiveness.

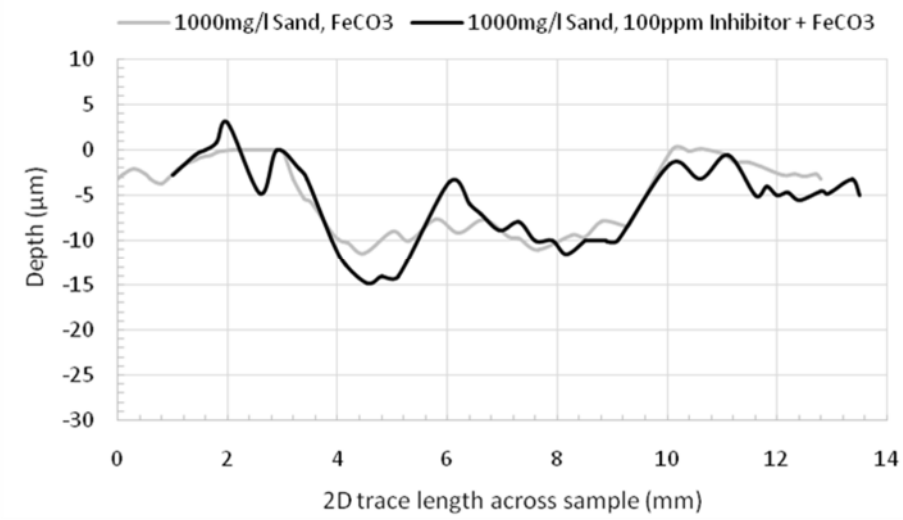

Figure 12: 2D profiles for API 5L X65 erosion-corrosion samples after cleaning. Tests are with and without the application of 100 ppm corrosion inhibitor on initially $FeCO_3$ pre-filmed X65 steel samples. Test Conditions: 15 m/s, 25℃, pH 4.7, 1000 mg/L sand in a CO_2-saturated 3.5 wt.%NaCl solution at 1 bar total pressure.

4. Conclusions

This work focused on the evaluation of $FeCO_3$ corrosion product to provide protection to carbon steel substrates in CO_2-containing flow-induced corrosion and erosion-corrosion environments, both in the absence and presence of a commercial corrosion inhibitor. As a result of this work, the main findings were:

- The sole presence of the $FeCO_3$ layer on carbon (i.e. in the absence of chemical inhibition) can assist in the reduction of the corrosion component of degradation in both the flow-induced and erosion-corrosion environments considered in this work.
- Although the erosion component recorded under uninhibited erosion-corrosion conditions was relatively high for pre-filmed carbon steel samples (as it comprises of the removal of the $FeCO_3$ layer as well as damage to the steel substrate), profilometry analysis revealed that the layer does afford some erosion protection to the steel substrate, reducing the total wear scar depth at the centre of the sample from ~20 to ~10 μm based on 6 h experiments in the absence of inhibitor.
- Full removal of $FeCO_3$ was observed at the centre of the carbon steel sample in erosion-corrosion conditions with no inhibitor within 6 h, indicating that although protection was afforded, it was not sustained throughout the entire test.
- The application of a commercial corrosion inhibitor was shown to work synergistically with the $FeCO_3$ layer to reduce the corrosion component of degradation in flow-induced corrosion and erosion-corrosion environments.
- The use of the inhibitor improved the resilience of the $FeCO_3$ layer to either chemical or hydrodynamic removal (or both) in flow-induced corrosion environments.

5. Acknowledgements

The authors would like to acknowledge the support provided by CNPq, ANP and Shell.

6. References

[1] T. C. Almeida, M. C. E. Bandeira, R. M. Moreira, O. R. Mattos, New insights on the role of CO_2 in the mechanism of carbon steel corrosion. Corros. Sci., 120 (2017) 239–250.

[2] H. Marchebois, J. Leyer, B. Orlans-Joliet, Ssc Performance Of A Super 13% Cr Martensitic Stainless Steel For Octg: Three-Dimensional Fitness-For-Purpose Mapping According To PH_2S, Ph And Chloride Content, NACE Corros.(2007) (Paper ID: NACE-07090)

[3] K. D. Efird, E. J. Wright, J. A. Boros, T. G. Hailey, Correlation of Steel Corrosion in Pipe Flow with Jet Impingement and Rotating Cylinder Tests. Corrosion, 1993; 49 (12) 992-1003.

[4] R. Barker, A. Neville, X. Hu, S. Cushnaghan, Evaluating Inhibitor Performance in CO_2-Saturated Erosion-Corrosion Environments. Corrosion, 2015; 71(1) 14-29.

[5] X. Hu, R. Barker, A. Neville, A. Gnanavelu, Case study on erosion-corrosion degradation of pipework located on an offshore oil and gas facility. Wear 271 (2011) 1295–1301.

[6] A. Akbar, X. Hu, C. Wang, A. Neville, The Influence of Flow Rate, Sand and Inhibitor On Iron Carbonate Scales Under Erosion-Corrosion Conditions Using A Submerged Impingement Jet, NACE Corros. (2012) (PAPER ID: NACE-2012-1396).

[7] S. Hassani, K. P. Roberts, S. Shirazi, J. R. Shadley, E. F. Rybicki, C. J. B. Joia, A New Approach for Predicting Inhibited Erosion-Corrosion in CO_2- saturated oil/brine Flow Condition, SPE (2012) (PAPER ID: SPE-1551136-MS).

[8] S. Ramachandran, Y. S. Ahn, V. Jovancicevic, J. Basset, Further Advances in the Development of Erosion Corrosion Inhibitors, NACE Corros. (2005) (PAPER ID: NACE-05292)

[9] A. Neville & C. Wang, Erosion-Corrosion Mitigation by Corrosion Inhibitors – An Assessment of Mechanisms. Wear 267 (2009) 195–203.

[10] R. Barker, X. Hu, A. Neville, S. Cushnaghan, Inhibition of Flow-Induced Corrosion and Erosion-Corrosion for Carbon Steel Pipe Work from an Offshore Oil and Gas Facility. Corrosion 2013; 69(2) 193-203.

[11] A. Dugstad, Mechanism of Protective Film Formation During CO_2 Corrosion of Carbon Steel, NACE Corros. (1998) (PAPER ID: NACE-98031)

[12] A. Palencsár, E. Gulbrandsen, K. Kosorú, Corrosion Inhibition under $FeCO_3$-forming Conditions at Elevated Temperatures, SPE (2014) (PAPER ID: SPE-169614-MS)

[13] S. M. Yaakob, M. C. Ismail, Corrosion inhibitor performance with presence of $FeCO_3$ film in CO_2 corrosion environment under fluid flow effect, Adv. Mat. Res.789(2013) 507-510.

[14] O. O. Ige, L. E. Umoru, Effects of shear stress on the erosion-corrosion behaviour of X-65 carbon steel: A combined mass-loss and profilometry study. Tribol. Int. 94 (2016) 155–164.

[15] ASTM, STANDARD G1-03, Standard practice for preparing, cleaning, and evaluating corrosion test specimens. ASTM International, 2003.

[16] A. J. McMahon, J. W. Martin, L. Harris, Effects of Sand and Interfacial Adsorption Loss on Corrosion Inhibitor Efficiency, NACE Corros. (2005) (PAPER ID: NACE-05274)

[17] I. Finnie, Some observations on the erosion of ductile metals. Wear, 19 (1972) 81-90.

[18] F. Pessu, R. Barker, A. Neville, The influence of pH on localized corrosion behavior of X65 carbon steel in CO_2-saturated brines. Corrosion, 2015; 71 (12) 1452-1466.